Chemical Science

ROYAL SOCIETY OF CHEMISTRY

EDGE ARTICLE

View Article Online
View Journal | View Issue

Cite this: *Chem. Sci.*, 2024, **15**, 10867

All publication charges for this article have been paid for by the Royal Society of Chemistry

Photophysics and photochemistry of thermally activated delayed fluorescence emitters based on the multiple resonance effect: transient optical and electron paramagnetic resonance studies†

Xi Chen, ‡[a] Lei Sun,‡[bc] Andrey A. Sukhanov,‡[d] Sandra Doria,‡[ef] Laura Bussotti,[e] Jianzhang Zhao, *[a] Haijun Xu, *[bc] Bernhard Dick, *[g] Violeta K. Voronkova*[d] and Mariangela Di Donato *[ef]

The photochemistry of two representative thermally activated delayed fluorescence (TADF) emitters based on the multiple resonance effect (MRE) (**DABNA-1** and **DtBuCzB**) was studied. No significant TADF was observed in fluid solution, although the compounds have a long-lived triplet state (*ca.* 30 μs). We found that these planar boron molecules bind with Lewis bases, *e.g.*, 4-dimethylaminopyridine (**DMAP**) or an *N*-heterocyclic carbene (**NHC**). A new blue-shifted absorption band centered at 368 nm was observed for **DtBuCzB** upon formation of the adduct; however, the fluorescence of the adduct is the same as that of the free **DtBuCzB**. We propose that photo-dissociation occurs for the **DtBuCzB-DMAP** adduct, which is confirmed by femtosecond transient absorption spectra, implying that fluorescence originates from **DtBuCzB** produced by photo-dissociation; the subsequent *in situ* re-binding was observed with nanosecdon transient absorption spectroscopy. No photo-dissociation was observed for the **NHC** adduct. Time-resolved electron paramagnetic resonance (TREPR) spectra show that the triplet states of **DABNA-1** and **DtBuCzB** have similar zero field splitting (ZFS) parameters (D = 1450 MHz). Theoretical studies show that the slow ISC is due to small SOC and weak Herzberg–Teller coupling, although the S_1/T_1 energy gap is small (0.14 eV), which rationalizes the lack of TADF.

Received 16th April 2024
Accepted 31st May 2024

DOI: 10.1039/d4sc02513j

rsc.li/chemical-science

Introduction

Charge separation (CS) occurring in organic electron donor–acceptor (D–A) dyads upon photoexcitation is of particular interest, because of its significance in fundamental photochemistry studies,[1,2] as well as in photovoltaics,[3–5] photocatalysis,[2,6–8] *etc.* CS and charge recombination (CR) are also involved in some novel organic optical materials; one example is electron D–A dyads showing thermally activated delayed fluorescence (TADF), which are promising emitters for organic light emitting diodes (OLEDs).[9–22]

In typical D–A type TADF emitters, discrete donor and acceptor units are connected *via* a linker, and the π-conjugation planes of the electron donor and acceptor units usually adopt an orthogonal geometry, making the electron exchange energy (J) of the CS states small. As a result, the ^{1}CS/^{3}CS state energy gap ($2J$) is reduced because of the poor molecular orbital overlap, which may facilitate the reverse intersystem crossing (rISC).[11,16,23–25] In this way, the triplet excitons can be harvested for electroluminescence, through repopulation of the emissive ^{1}CS state. The ISC mechanism operating in orthogonal dyads is often referred to as spin–orbit charge transfer (SOCT) ISC, since in these cases the electron spin angular momentum change occurring during ISC is off-set by the molecular orbital angular momentum change of the electron transfer.[26–29] Recently, we highlighted the critical role of dark states, such as the ^{3}LE (LE: localized excited state) and the ^{3}CS states, in the TADF process

[a]*State Key Laboratory of Fine Chemicals, Frontier Science Center for Smart Materials, School of Chemical Engineering, Dalian University of Technology, Dalian 116024, P. R. China. E-mail: zhaojzh@dlut.edu.cn*

[b]*Jiangsu Co-Innovation Center of Efficient Processing and Utilization of Forest Resources, Key Laboratory of Forestry Genetics & Biotechnology of Ministry of Education, Jiangsu Provincial Key Lab for the Chemistry and Utilization of Agro-Forest Biomass, College of Chemical Engineering, Nanjing Forestry University, Nanjing, 210037, P. R. China. E-mail: xuhaijun@njfu.edu.cn*

[c]*School of Chemistry and Chemical Engineering, Henan Normal University, Xinxiang, 453002, China*

[d]*Zavoisky Physical-Technical Institute, FRC Kazan Scientific Center of RAS, Kazan 420029, Russia. E-mail: vio@kfti.knc.ru*

[e]*LENS (European Laboratory for Non-Linear Spectroscopy), Via N. Carrara 1, 50019 Sesto Fiorentino (FI), Italy. E-mail: didonato@lens.unifi.it*

[f]*ICCOM-CNR, Via Madonna del Piano 10-12, 50019, Sesto Fiorentino (FI), Italy*

[g]*Lehrstuhl für Physikalische Chemie, Institut für Physikalische und Theoretische Chemie, Universität Regensburg, Regensburg 93053, Germany. E-mail: Bernhard.Dick@chemie.uni-regensburg.de*

† Electronic supplementary information (ESI) available. See DOI: https://doi.org/10.1039/d4sc02513j

‡ These authors contributed equally to this work.

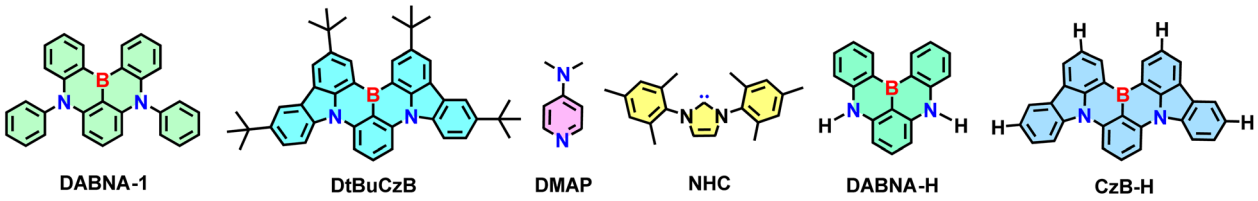

Scheme 1 Molecular structures of the MRE emitters **DtBuCzB**, **DABNA-1**, **CzB-H**, and **DABNA-H** used in calculations. The molecular structures of the Lewis bases **DMAP** and **NHC** used in the study are also presented.

of D–A dyads,[29–32] by using femtosecond and nanosecond transient absorption (fs/ns-TA) spectroscopy. Most of our measurements experimentally supported the three-state theoretical model, invoked for D–A TADF emitters, according to which the delayed fluorescence is believed to occur through a spin-vibronic coupling mechanism.[29–34]

Conventional D–A TADF emitters for OLED applications suffer from some limitations. For instance, the spatial separation between the HOMO and LUMO, usually respectively confined on the donor and acceptor, leads to poor radiative decay from the ^{1}CS state. Furthermore, the CS character of the emissive state leads to a large fluorescence bandwidth, which is detrimental for applications for information display purposes.[35] One alternative to the conventional D–A TADF emitters is to obtain systems with an emissive S_1 state presenting reduced CS character. Unfortunately, it is challenging to maintain a small electron exchange energy while minimizing the molecular orbital spatial separation, because the J magnitude increases with increasing orbital overlapping. Recently, some novel molecular structure has been developed to address this challenge, and TADF emitters based on the multiple resonance effect (MRE) have been proposed.[35–48]

In these compounds, electron-deficient and electron-rich atoms, such as boron and nitrogen, are positioned alternatively, in a way that the HOMO and LUMO of the molecule are confined on different atoms. Since nitrogen exhibits the opposite resonance effect of boron, *para*-substitution relative to it can enhance the resonance effect and can significantly spatially separate the HOMO and LUMO without the need to introduce discrete electron donor and acceptor units in the molecular structures. These compounds have a small J and present a 'short-range' charge separation, in contrast to the conventional D–A TADF emitters, which instead present 'long range' change separation. TADF emitters based on the MRE have large $S_1 \rightarrow S_0$ radiative transition oscillator strength and narrow emission bands, because of their rigid π-conjugation frameworks and their non-conventional HOMO–LUMO separation. Their application in OLED devices has been extensively studied and promising results have been obtained;[44,46,49–51] nevertheless their photophysical processes are not completely understood. Many reports can be found in the literature concerning the confinement of the excited state wave functions of conventional D–A TADF emitters, especially in their triplet states. Indeed, for these systems, both the ^{3}LE and ^{3}CS states have been well characterized by transient optical spectroscopic methods,[25,27,29–31,52–55] as well as with pulsed laser excited time-resolved electron paramagnetic resonance (TREPR) spectroscopy.[56–59] For the conventional CS state, the zero field splitting (ZFS) D parameter of the ^{3}CS state is much smaller than that of the ^{3}LE state of the chromophore,[1,27,60–62] because the ZFS D parameter depends on the electron spin–spin dipolar interaction magnitude, and it is related to the distance between the two electrons. However, little information is available for the spin–spin dipolar interaction magnitude of the triplet excited state of MRE emitters.[35] Moreover, the central B atom of these molecules should behave like a Lewis acid, but little is known about the experimental manifestation of this property, and the relation between the Lewis acidity and the TADF properties.

Herein we selected two representative MRE-TADF emitters, *i.e.*, **DABNA-1** and **DtBuCzB** (Scheme 1). Both compounds have a triangulene core incorporating *ortho*-substituted boron and nitrogen atoms to promote the MRE. **DABNA-1** is one of the first reported MRE TADF emitters[37] and **DtBuCzB** was also reported for application in OLED devices.[63] For both compounds, delayed fluorescence was observed when dispersed in films with 3,3′-bis(*N*-carbazolyl)1,1′-biphenyl (mCBP) as the host material, showing a lifetime of 68.8 μs.[63] However, their excited state dynamics was not studied in detail. In this paper we analyzed their photophysical properties using fs/ns-TA spectroscopic methods, as well as TREPR spectroscopy. The Lewis acidity of the boron center was characterized through the formation of Lewis acid-adducts with pyridine derivatives and with a typical *N*-heterocyclic carbene.

Results and discussion

Experimental

Molecular structure designing rationales. We selected two representative MRE-TADF emitters, **DABNA-1** and **DtBuCzB**. Two Lewis bases, 4-dimethylaminopyridine (**DMAP**) and a *N*-heterocyclic carbene (**NHC**), 1,3-bis(2,4,6-trimethylphenyl)-1,3-dihydro-2*H*-imidazol-2-ylidene (Scheme 1) were used for the binding study. It was shown that the OLED devices fabricated with these two emitters have high electroluminescence efficiency.[37,63] The fs-TA spectra of a molecule very similar to **DABNA-1** have been reported previously.[64] Some theoretical studies have also been carried out for **DABNA-1**.[39,65–67]

UV-vis absorption and fluorescence emission studies. The UV-vis absorption spectra of the MRE emitters **DABNA-1** and **DtBuCzB** are presented in Fig. 1. The two compounds show moderate absorption below 350 nm ($\varepsilon = 1.5 \times 10^4$ M^{-1} cm^{-1} at 332 nm), and a strong, sharp absorption band centered at

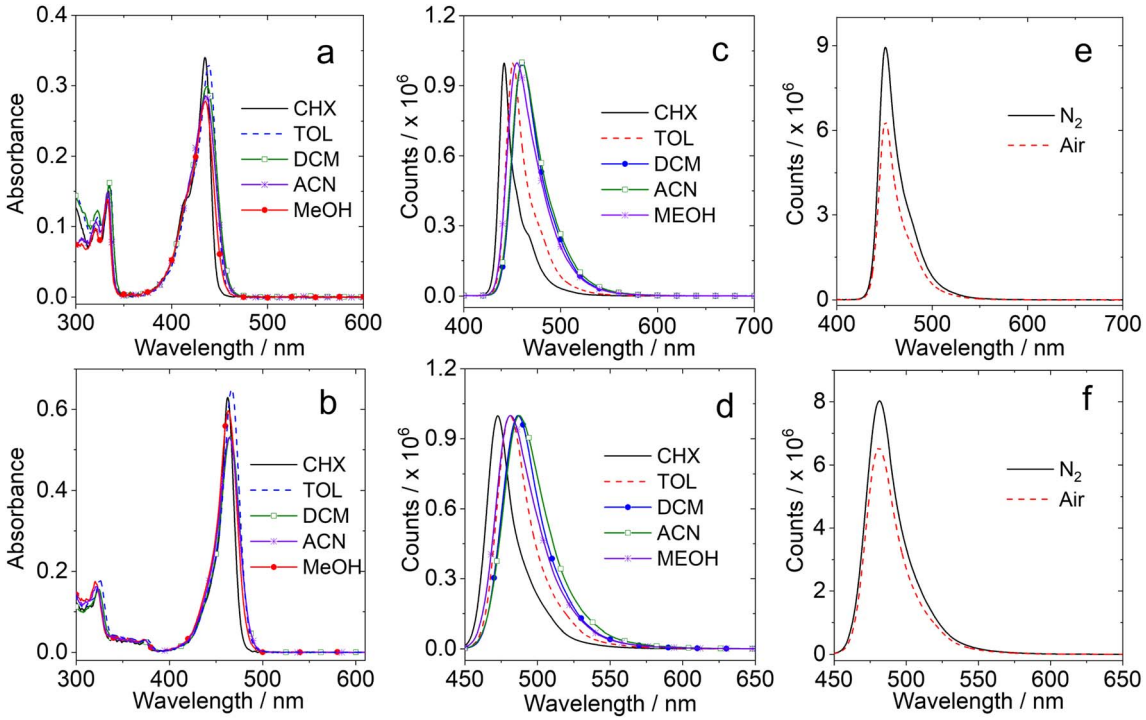

Fig. 1 UV-vis absorption spectra of (a) **DABNA-1** and (b) **DtBuCzB** in cyclohexane (CHX), toluene (TOL), dichloromethane (DCM), acetonitrile (ACN), and methanol (MeOH), $c = 1.0 \times 10^{-5}$ M. Normalized fluorescence spectra of (c) **DABNA-1** ($\lambda_{ex} = 335$ nm) and (d) **DtBuCzB**, ($\lambda_{ex} = 440$ nm) in different solvents, and (e) **DABNA-1** and (f) **DtBuCzB** in toluene in different atmospheres. Optically matched solutions were used, $A \approx 0.10$.

438 nm ($\varepsilon = 3.3 \times 10^4$ M^{-1} cm^{-1}) for **DABNA-1** and 467 nm ($\varepsilon = 6.5 \times 10^4$ M^{-1} cm^{-1}) for **DtBuCzB** (Table 1).

The full width at half maximum (FWHM) of the absorption band is *ca.* 983 cm^{-1} for **DABNA-1** and 1382 cm^{-1} for **DtBuCzB**. Both compounds do not present charge transfer (CT) absorption bands, although the electron rich and deficient atoms are alternatively positioned.[68] The UV-vis absorption spectra of **DABNA-1** and **DtBuCzB** remain the same in different solvents, indicating that the ground state dipole moment is small.[69]

The fluorescence spectra of the compounds are shown in Fig. 1c and d. The fluorescence emission bands are quite narrow and only show minor changes in solvents with different polarities, as observed for other MRE TADF emitters,[65,70] indicating that the emissive S_1 state has no conventional intramolecular charge transfer (ICT) character.[14,15,71,72]

The fluorescence intensity under N_2 and air atmospheres are similar (Fig. 1e and f), different from typical D–A TADF emitters, which usually show stronger fluorescence under a N_2 atmosphere because triplet states, that are strongly quenched by dioxygen (O_2), are involved in the TADF process. The results observed for **DABNA-1** and **DtBuCzB** indicate either that their excited state lifetime is short (less than a few dozens of ns) or that the TADF is not significant. Recently it was proposed that some MRE compounds, such as **DABNA-1**, do not show TADF behavior in solution, but only in particular solid matrices,[40] although they have a small singlet/triplet energy gap $\Delta E_{S_1/T_1} =$ 0.14–0.18 eV.[37]

Organic boron materials are usually highly reactive and have to be stabilized by steric protection. Planar organic boron compounds with constrained molecular geometry are more

Table 1 Photophysical parameters of the compounds

	λ_{abs} [a] (nm)	ε [b]	λ_{em} [c] (nm)	τ_{PF} [d] (ns)	τ_{DF} [e] (ns)	τ_T [f] (μs)	Φ_F [g] (%)	Φ_Δ [h] (%)
DABNA-1	439	3.3	451	5.7	—[i]	34.3	67.1/74.9/83.0/68.7/68.0	10.8
DABNA-1-DMAP	368	1.5	452	5.8	—[i]	—[i]	89.7	0.0
DABNA-1-NHC	439	3.0	451	5.7	—[i]	—[i]	12.0	0.0
DtBuCzB	466	6.5	481	4.9	—[i]	38.2	83.7/98.5/97.2/92.0/85.2	1.0
DtBuCzB-DMAP	368	1.5	481	4.5	—[i]	13.9	85.1	0.0
DtBuCzB-NHC	357	3.4	383	5.4	136	2.3	2.0	0.0

[a] In TOL. Maximal UV-vis absorption wavelength, $c = 1.0 \times 10^{-5}$ M, 20 °C. [b] Molar absorption coefficient at absorption maxima, ε: 10^4 M^{-1} cm^{-1}. [c] Emission wavelength. [d] Fluorescence lifetime, $\lambda_{ex} = 340$ nm. [e] Delayed fluorescence lifetime, $\lambda_{ex} = 340$ nm. [f] Triplet state lifetime. [g] Fluorescence quantum yields determined ($\lambda_{ex} = 333$ nm) for **DABNA-1** and **DtBuCzB** in CHX/TOL/DCM/ACN/MeOH, respectively. [h] Singlet oxygen quantum yields, $Ru(bpy)_3[PF_6]_2$ was used as the standard compound ($\Phi_\Delta = 57\%$ in DCM), $\lambda_{ex} = 340$ nm. [i] Not observed.

stable because of structural constraints. Indeed, the rigidly fixed cyclic skeleton around the boron atom would retard decomposition through the reactions with Lewis basic species, because of the destabilization of a tetra-coordinated intermediate and/or prevention of C–B bond cleavage from the intermediate by the chelating effect.[73]

It should be noted that the boron centers of both **DABNA-1** and **DtBuCzB** have Lewis acid character and should be able to bind with Lewis bases. The binding can induce notable perturbation of the MRE character, without modification of the molecular structure. The binding with a Lewis base such as **DMAP**, inducing the formation of a B–N dative bond, will eliminate the MRE, because of the occupation of the vacant p-orbital of the boron atoms. Recently it was shown that **DtBuCzB** and 5,9-dioxa-13*b*-boranaphtho[3,2,1-*de*]anthracene (**DOBNA**) can interact with Lewis bases such as pyridine, **DMAP**, and the fluoride ion (F^-). **DtBuCzB** was used as a F^- probe, because of its very high binding constant with F^- of 1.16×10^5 M^{-1}.[74]

We analyzed the UV-vis absorption spectral changes of the MRE emitters upon binding with **DMAP** and **NHC** (Fig. 2). Upon incremental addition of **DMAP** into the solution of **DtBuCzB** in toluene, the strong absorption band of the native **DtBuCzB** centered at 467 nm as well as the minor band centered at 325 nm decreased in intensity, and a new band centered at 368 nm developed (Fig. 2a). This result is literally the same as the UV-vis evolution upon binding with F^- anions.[74] Similar results were observed upon addition of **NHC** (Fig. 2d). The color change in the solution upon formation of the adduct is visible to the naked eye (Fig. 2f).

Previously, similar changes were observed for the binding of planar organoboron compounds with Lewis bases such as **DMAP**.[75–77] The Gibbs free energy change ($\Delta G°$) of the binding process with **DMAP** is -21.1 kJ mol^{-1} (Table 2). Similar results were observed for **DABNA-1**, although its binding constant is smaller, with $K = (1.06 \pm 0.001) \times 10^2$ M^{-1}. Previously it was found that **DtBuCzB** can bind with F anions with a higher binding constant (1.16×10^5 M^{-1}).[74] Some analogues containing an O atom instead of N atoms, showing lower electron density in the aromatic rings compared to **DABNA-1**, have a stronger binding constant with DMAP (4.29×10^4 M^{-1}) compared to **DABNA-1**.[78,79] **DABNA-1** cannot bind with **NHC**, showing no significant changes in the UV-vis absorption and fluorescence spectra even upon the addition of 500 equivalents of **NHC**. For the adduct of **DtBuCzB** with **NHC**, a blue-shifted emission band centered at 383 nm was observed, along with the emission of the native **DtBuCzB** (Fig. 2e). The emission band at 383 nm is attributed to the adduct, while that centered at 481 nm is assigned to the free **DtBuCzB**. Note the binding of **DtBuCzB** with **NHC** is slightly tighter than that with **DMAP** (Table 2). The evolution of the fluorescence spectra is similar to

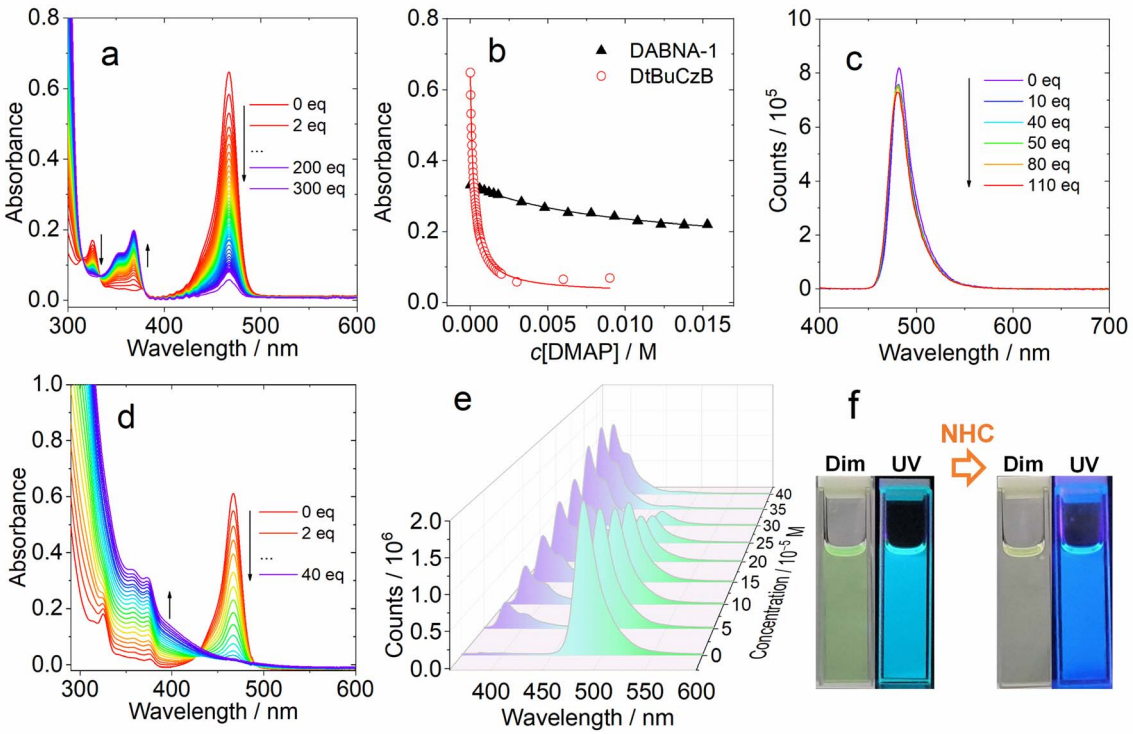

Fig. 2 (a) Evolution of the UV-vis absorption spectra of **DtBuCzB** with an incremental amount of **DMAP** added. (b) The titration isotherms of **DABNA-1** (monitored at 439 nm) and **DtBuCzB** (monitored at 467 nm). The solid lines are the fitting for the binding constants of **DABNA-1** or **DtBuCzB** toward **DMAP**. (c) Fluorescence spectra of **DtBuCzB** with an incremental amount of **DMAP** added. (d) UV-vis absorption spectra of **DtBuCzB** with an incremental amount of **NHC** added. (e) Fluorescence spectra of **DtBuCzB** with different concentrations of **NHC** in toluene, λ_{ex} = 333 nm (isosbestic point of the UV-vis absorption spectra). (f) The digital photographs of the solution of **DtBuCzB** upon addition of **NHC** (40 eq.) under dim light and UV light (365 nm) illumination, respectively. $c = 1.0 \times 10^{-5}$ M, 20 °C.

Table 2 Binding constant and the change in Gibbs free energy of the compounds[a]

	DABNA-1		DtBuCzB	
	K (M^{-1})	ΔG (kJ mol^{-1})	K (M^{-1})	ΔG (kJ mol^{-1})
DMAP	$(1.06 \pm 0.001) \times 10^2$	−11.55	$(4.51 \pm 0.007) \times 10^3$	−20.85
NHC	—[b]	—[b]	$(5.06 \pm 0.03) \times 10^3$	−21.13
DABCO	—[b]	—[b]	$(4.01 \pm 0.006) \times 10^2$	−14.85
2-Methylpyridine	—[b]	—[b]	—[b]	—[b]

[a] $\Delta G = -RT \ln K$, $R \approx 8.314$ J mol^{-1} K^{-1}, $T = 298$ K. [b] Values are so small as to be negligible.

that found for analogues based on boron-containing dioxygen-bridged molecules.[78]

Interestingly, we did not observe any variation of the fluorescence of **DtBuCzB** upon incremental addition of **DMAP** (Fig. 2c), when exciting the solutions at the isosbestic point (333 nm) of the UV-vis absorption spectrum of the mixture. This observation is unexpected, considering the substantial changes observed in the UV-vis absorption spectrum of the mixture (Fig. 2a), which indicate an efficient formation of the Lewis acid–base adduct. A corresponding decrease in fluorescence intensity would be expected, unless the **DtBuCzB-DMAP** complex would have exactly the same fluorescence as the free **DtBuCzB**, which is unlikely. We thus propose that photodissociation may occur upon photoexcitation of the adduct, and that the observed fluorescence is emitted from the photo-released free **DtBuCzB**.[80] Previously, a similar photodissociation was observed for a planar organoboron compound coordinated with a Lewis base (these compounds have no MRE properties).[76] Since the ISC of **DtBuCzB** is not efficient, we assume that photodissociation occurs at the singlet excited state (see later section for the ultrafast transient absorption studies).[75] This is different from the scenario of the binding of **DtBuCzB** with F^- anions, for which the fluorescence is strongly quenched,[74] possibly because of tight binding, avoiding the photodissociation of the adduct. The binding of the MRE emitters with other Lewis bases such as 1,4-diazabicyclo[2.2.2]octane (DABCO) and 2-methylpyridine wasere also studied, and smaller binding constants were observed.

Previously it was found that photodissociation of the adduct formed between a planar trinaphthylborane, having a partially fused structure, and a Lewis base pyridine, generated a dual emission, due to both the adduct and photodissociated borane.[75] In our case, although the binding constant is similar, only the fluorescence of the photogenerated **DtBuCzB** was detected. The prerequisite for emission of the adduct would be a tight binding. For instance, in the case of the adduct of a planar trinaphthylborane with **DMAP**,[75] presenting a very high binding constant of $(6.6 \pm 1.3) \times 10^6$ M^{-1}, no photodissociation was observed.[75] The extension of the π-conjugation framework of the MRE TADF emitters **DABNA-1** and **DtBuCzB** may decrease the Lewis acidity of the boron center, thus decreasing the binding constants.[81]

These examples demonstrate that the occurrence of photodissociation is strongly dependent on the magnitude of the binding constants. Nevertheless, photodissociation was also not observed in the case of an organoboron-phosphine B–P adduct, although its binding constant, $K = 61$ M^{-1},[76] is smaller. It was also proposed that the photo-generated borane could rebind with pyridine, but this possibility was not confirmed experimentally, for instance by using ns-TA spectroscopy.[75]

The binding of borane with Lewis bases has been used for controlling the fluorescence,[82–84] and for dynamic modulation of (anti)aromaticity and diradical character of organic diradicaloids.[81] For our system, the adduct is formed at room temperature, while for the previously reported borane and phosphine ligand, the adduct can only be formed at low temperature (<270 K).[76] In order to quantify the Lewis basicity of the boranes, we carried out Gutmann–Beckett measurements, using $Et_3P{=}O$ to monitor the shift of the ^{31}P NMR signal.[76] For **DABNA-1**, the chemical shifts changed slightly with $Et_3P{=}O$ (*e.g.* from 52.78 ppm of the planar triangonal to 54.92 ppm of the sp^3 hybridized boron center, Fig. S6†), while they changed to a larger extent for **DtBuCzB** (*e.g.* from 52.78 ppm of the planar triangonal to 55.67 ppm of the sp^3 hybridized boron center, Fig. S7†). For previous compounds the chemical shift changes of ^{31}P after complexation with planar boron compounds were found to be $\Delta P = 0.03$ and 3.56 ppm.[76]

Based on the ns-TA spectral study (see later section), we propose that for the adduct formed between **DtBuCzB** and **NHC**, the fluorescence centered at *ca.* 480 nm is due to the residual free **DtBuCzB**, and not due to photodissociation of the Lewis acid–base adduct. This agrees with the tight binding between **DtBuCzB** and the **NHC** Lewis base. This result is similar to the previously reported binding between planarized borane and **DMAP**.[75] The adduct of an oxygen-bridged planarized triphenylborane with **DMAP**, showing binding constant of $K = (6.6 \pm 1.9) \times 10^7$ M^{-1}, exhibits very weak fluorescence at room temperature.[80]

We further measured the fluorescence lifetimes of the compounds in deaerated solutions (Fig. 3 and S16†). The luminescence decay trace of **DtBuCzB** in deaerated toluene has biexponential character (5.9 ns/99.1%, 244 ns/0.9%, Fig. 3a). Similar results were observed with the solution under an air atmosphere (4.9 ns/99.7%, 506 ns/0.3%). Biexponential decay traces were also observed for **DABNA-1** (Fig. 3d). Considering that the long living component of the fluorescence decay is not quenched by air, we conclude that TADF is not significant for **DtBuCzB** and **DABNA-1** in toluene.

We attribute the long-lived signal to instrument noise. The fluorescence lifetime of **DABNA-1** was reported to be 9.5 ns (in

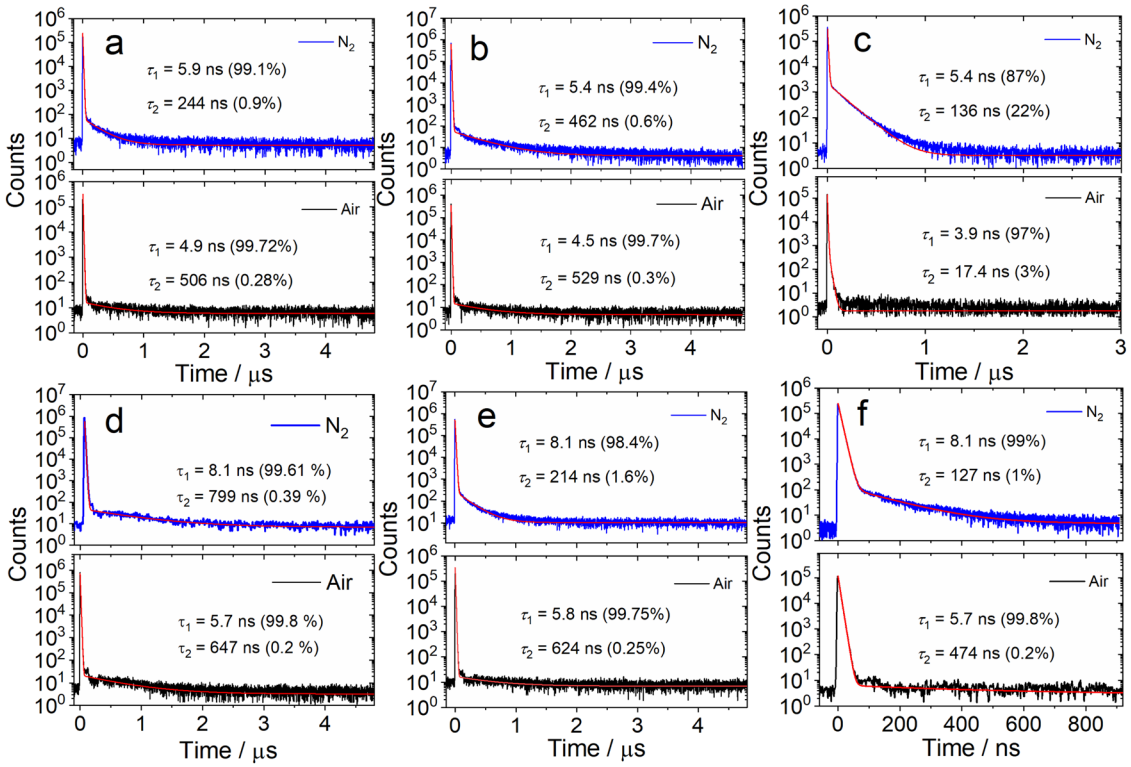

Fig. 3 Fluorescence decay traces of (a) **DtBuCzB** (480 nm); (b) **DtBuCzB** with **DMAP** (481 nm); (c) **DtBuCzB** with **NHC** (388 nm); (d) **DABNA-1** (450 nm); (e) **DABNA-1** with **DMAP** (450 nm); (f) **DABNA-1** with **NHC** (450 nm) in different atmospheres in toluene. Excited with a picosecond pulsed laser, $\lambda_{ex} = 340$ nm, $c = 1.0 \times 10^{-5}$ M, 20 °C.

DCM, at a concentration of 2×10^{-5} M),[37] while TADF was only observed for **DABNA-1** in the doped films in the hole transfer material of 3,3-di(9*H*-carbazol-9-yl)biphenyl (mCBP. 1W%), with the prompt and delayed fluorescence lifetimes of 8.8 ns and 93.7 μs, respectively.[37] Recently Chou *et al.* proposed that TADF may result from the intermolecular interaction of these MRE-TADF emitters with the host materials in the OLED devices.[40]

We also studied the fluorescence lifetime of the adducts (Fig. 3b and e). For **DtBuCzB**, the decay trace of the adduct with **DMAP** shows biexponential character in toluene under a N_2 atmosphere (5.4 ns/99.4%, 462 ns/0.6%, Fig. 3b). Similar results were observed for the aerated solution (4.5 ns/99.7%, 529 ns/0.3%), as well as for the adduct of **DABNA-1** with **DMAP** (Fig. 3e), indicating that there is also no significant TADF for the adducts of **DtBuCzB** and **DABNA-1** with **DMAP**. Interestingly, the **DtBuCzB**/**NHC** adduct shows significant TADF, and a biexponential fluorescence decay trace was observed (Fig. 3c), with lifetimes of 5.4 ns (87%)/136 ns (22%). In the case of the adduct of **DABNA-1** with **NHC**, TADF is not observed, and the fluorescence has a biexponential decay both under a N_2 atmosphere (8.1 ns/99%, 127 ns/1%) and in air (5.7 ns/99.8%, 474 ns/0.2%) (Fig. 3f).

We further investigated the luminescence properties of the compounds at low temperatures, measuring the photoluminescence spectra of **DtBuCzB** and **DABNA-1** in a frozen solution of 2-methyltetrahydrofuran (Fig. 4) and 2-methyltetrahydrofuran/iodoethane (2 : 1, v/v). At 77 K the maximum of the phosphorescence bands are centered at 481 nm and 508 nm, respectively (Fig. S20†). The triplet excited state energy of **DtBuCzB** (2.56 eV) and **DABNA-1** (2.72 eV) is obtained by multi-peak fit analysis of the phosphorescence spectra, and results similar to the literature values are obtained (2.53 eV and 2.59 eV).[37,63] Moreover, we found that the luminescence spectra of **DtBuCzB** and **DABNA-1** in the presence of **DMAP** are blue shifted by 100 nm and 50 nm at 77 K (Fig. 4), implying that at low temperature we only observed the emission of the adduct since photodissociation is substantially suppressed.[75]

Femtosecond transient absorption (fs-TA) spectroscopy. The excited state dynamics of both **DABNA-1** and **DtBuCzB** was probed by measuring their transient absorption spectra with sub-ps time resolution (Fig. 5). The measurements were performed in toluene and the two compounds were photoexcited at 400 nm and 340 nm, respectively. The data were subjected to singular value decomposition (SVD) and global fitting, using a linear unidirectional decay scheme.

Selected transient absorption spectra and the evolution associated difference spectra (EADS) obtained from global analysis are reported in Fig. 5. While the transient absorption spectra of conventional TADF emitters have been extensively studied,[52,85] the analysis of the excited state dynamics of MRE compounds is rare. The fs-TA spectra of an analogue of **DABNA-1** were recently reported, and the results closely match those presented in Fig. 5a.[64] In the literature, **DABNA-1** was excited at

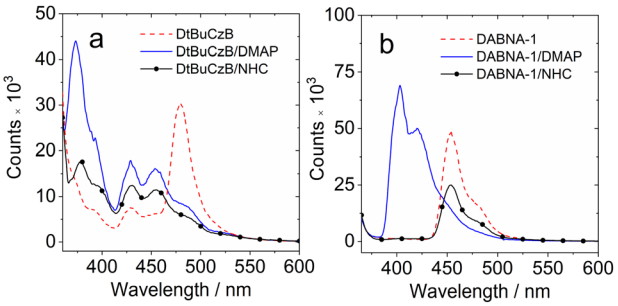

Fig. 4 Luminescence spectra of the compounds and the adducts in a frozen solution of (a) **DtBuCzB** alone, and in the presence of **DMAP** (50 eq.) or **NHC** (50 eq.) and (b) **DABNA-1** alone and in the presence of **DMAP** (50 eq.) and **NHC** (50 eq.) in 2-methyltetrahydrofuran at 77 K. Excited with a picosecond pulsed laser (λ_{ex} = 340 nm), c = 1.0 × 10^{-4} M.

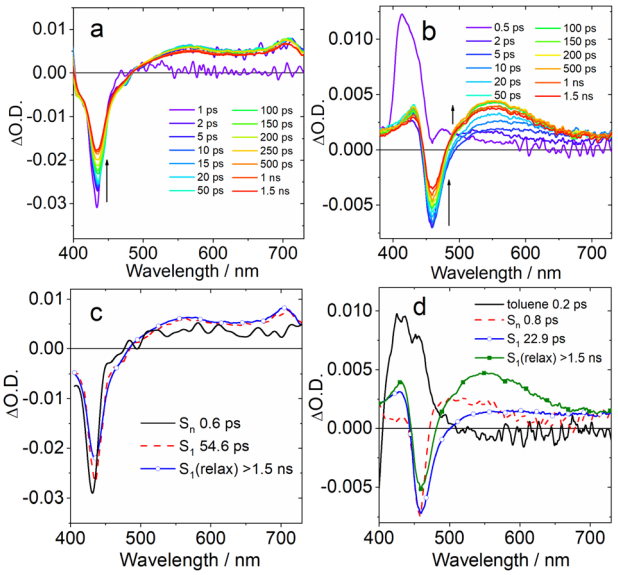

Fig. 5 Fs-TA spectra recorded in toluene for (a) **DABNA-1** excited at 400 nm and (b) **DtBuCzB** excited at 340 nm. Panels (c) and (d) present the EADS obtained from global analysis of the transient absorption data.

330 nm, and a rapid internal conversion (IC) from the initially populated S_n to the S_1 state was observed.

Upon excitation at 400 nm, the S_1 state is directly accessed. A negative band peaked at about 430 nm is observed immediately after excitation (Fig. 5c), ascribed to the convolution of ground state bleaching (GSB) and stimulated emission (SE), which can't be spectrally resolved because of the small Stokes shift. The transient spectrum evolves on a very fast timescale of 0.6 ps: the negative band broadens on its red side and a positive excited state absorption (ESA) band develops in the 500–700 nm region. We attribute this evolution to a fast solvent induced relaxation of the S_1 state. In the following 54 ps, a second evolution is noticed, mainly consisting in a further slight red shift of the SE band and an overall intensity decrease of the negative signal.

Previous investigations on a similar compound, both in the visible and IR regions,[67] attributed an evolution observed on a similar timescale to structural relaxation, consisting in a planarization of the molecule in the excited state. The assignment is based on a theoretical analysis. In agreement with the previous report, we interpret the evolution between the second and third EADS in a similar way. The final spectral component does not decay on the investigated timescale (1.5 ns).

The transient spectra of **DtBuCzB** are similar to those of **DABNA-1** (Fig. 5b). In this case the sample was excited at 340 nm, thus reaching a higher energy excited state. The intense positive signal observed at a very fast time scale and decaying in about 200 fs is attributed to a solvent response following excitation with UV light (dashed line in Fig. 5d). The following spectral component (black continuous line in Fig. 5d) shows a negative signal peaked at about 458 nm, assigned to GSB, and a positive ESA in the 470–600 nm range. Stimulated emission is not observed on a very fast timescale, since the sample still has to relax towards the S_1 emissive state. This process occurs in about 0.8 ps, as shown by the broadening of the negative signal on its red side, caused by the SE build up, the red shift and broadening of the ESA band and the appearance of a second ESA peak at about 430 nm. In the following evolution, occurring in about 22 ps, the red-shifted ESA signal increases in intensity, and the negative GSB/SE signal slightly recovers. Analogous with what was discussed in the case of **DABNA-1**, we tentatively assign this evolution to a structural relaxation, possibly associated with the planarization of the molecule. Also in this case, the final spectral component lives longer than the timescale accessed with this measurement.

We furthermore studied the photodissociation dynamics of the adducts formed by **DABNA-1** and **DtBuCzB** with **DMAP** (Fig. 6). The transient spectra of the adduct **DABNA-1/DMAP** are very similar to those of the isolated **DABNA-1**, and also upon the addition of a great excess of **DMAP** in solution (Fig. S25†), except for some changes in the time constants describing the photodynamics (Fig. S23†). For the **DtBuCzB-DMAP** adduct, whose transient spectra and EADS are reported in Fig. 6, a more complex behaviour is observed.

Immediately after excitation, we observed an intense positive absorption signal, peaking at about 400 nm (Fig. 6a), which decays on a very fast timescale of about 200 fs, attributed to a fast response of the toluene solvent. The following spectral component, decaying in 25.0 ps, shows up as a very broad and

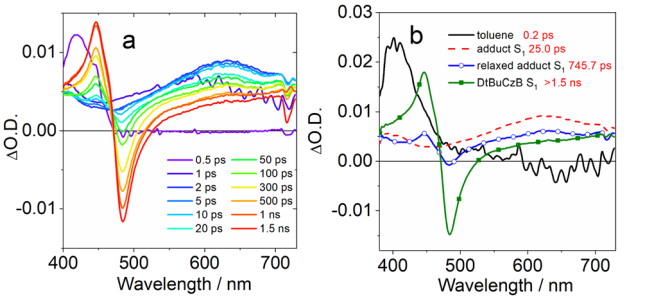

Fig. 6 (a) Fs-TA spectra of the **DtBuCzB-DMAP** (50 eq.) adduct recorded in toluene upon excitation at 370 nm. (b) The EADS obtained from global analysis of the transient absorption data.

weak positive signal, extending over the full probed spectral range, that we assign to the absorption of the **DtBuCzB-DMAP** adduct at the S_1 state. On this same timescale vibrational and structural relaxation is likely to occur as well. In the following evolution, a positive peak located at 446 nm and a negative peak at 483 nm start to appear superimposed on the broad positive signal of the adduct. The position of these signals closely matches the absorption and emission of **DtBuCzB** respectively, indicating the occurrence of photodissociation. The intensity of both bands further increases after 745 ps, indicating that the photodissociation has biexponential kinetics.

A possible explanation for biexponential photodissociation dynamics is the existence of different conformations of the adducts in solution, with some of them releasing **DMAP** more easily. The transient signals of the photogenerated **DtBuCzB** do not decay on the ns timescale, indicating that the re-binding of the photogenerated **DtBuCzB** and **DMAP** is slower. This is reasonable because this intermolecular process is diffusion-controlled, and can take up to microseconds in solution. We further studied the adduct formed by **DtBuCzB** with the carbene **NHC**. In this case photodissociation is not observed, because of the stronger binding between the two moieties. Indeed, the transient spectra only show a positive signal decaying on a fast timescale due to solvent response, and a very weak and broad band, similar to the second spectral component observed for the adduct **DtBuCzB/DMAP** (dotted red line in Fig. 6b), which does not decay on the ns timescale (Fig. S26†).

Nanosecond transient absorption (ns-TA) spectroscopy of the compounds. We analyzed the triplet state of the compounds, as well as that of their adducts with Lewis bases using ns-TA spectroscopy (Fig. 7). Upon pulsed laser excitation, a sharp ground state bleaching (GSB) band centered at 465 nm was observed for the pristine **DtBuCzB** (Fig. 7a), in agreement with the steady-state UV-vis absorption spectrum (Fig. 1a). A broad excited state absorption (ESA) band in the 500–850 nm range was also observed. The lifetime of the transient species was determined to be 38.2 μs (Fig. 7b). A GSB band centered at 440 nm and a broad ESA band in the 500–800 nm range were observed for **DABNA-1** (Fig. 7c). The lifetime of the transient species was determined to be 34.3 μs (Fig. 7d). The triplet state lifetime of **DABNA-1** was previously reported to be 100 μs.[67] It is possible that the triplet state was produced at a higher concentration in our case and that Triplet–Triplet Annihilation (TTA) occurred, shortening the triplet state lifetime. As previously mentioned, even if **DABNA-1** has a long-lived triplet state, no significant TADF is observed in solution at room temperatures (Fig. 4), indicating that the equilibrium between the triplet state and the emissive S_1 state is not efficient.

We then studied the dynamic behavior of the adducts of the MRE compounds with Lewis bases. In the case of **DtBuCzB** in the presence of an excess of **DMAP** a GSB band centered at 366 nm was observed, in agreement with its steady state absorption spectrum (Fig. 8a). Interestingly, a sharp positive absorption band centered at 465 nm was also observed. The position of this band corresponds very well to the steady state UV-vis absorption band of the free **DtBuCzB** (Fig. 1).

Based on the fluorescence study of **DtBuCzB** in the presence of **DMAP**, and the results of the ultrafast transient absorption measurements presented in the previous section, both indicating the occurrence of photo-dissociation of the bound **DMAP** (Fig. 2c), the sharp band centered at 465 nm is assigned to the photogenerated free **DtBuCzB** (Fig. 8a).

In the presence of excess **DMAP** in the mixture solution, the photo-generated free **DtBuCzB** becomes a 'transient' species,

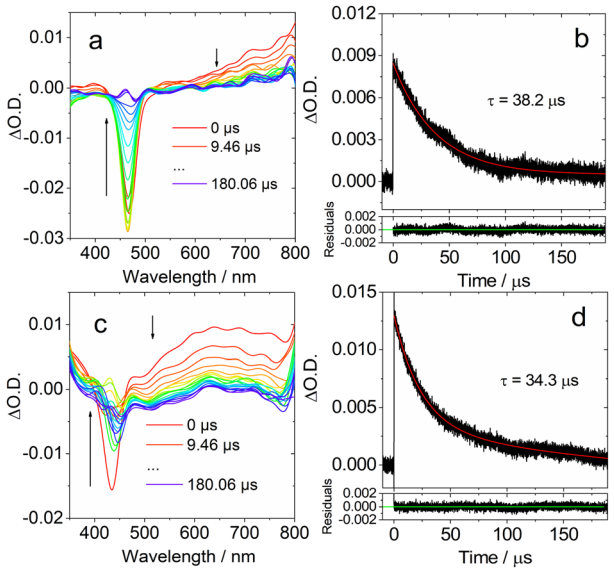

Fig. 7 Ns-TA spectra in DCM of (a) **DtBuCzB** and (c) **DABNA-1**. Decay traces of (b) **DtBuCzB** at 750 nm; (d) **DABNA-1** at 650 nm. Excited at 440 nm and 420 nm, respectively. $c = 2.0 \times 10^{-5}$ M, 20 °C.

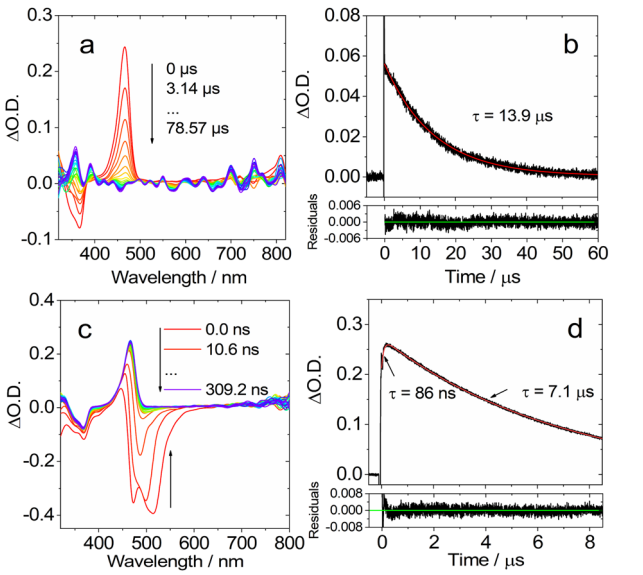

Fig. 8 Ns-TA spectra in toluene of **DtBuCzB** with 4-*N*,*N*-dimethylaminopyridine (**DMAP**. 50 eq.) added. (a) Recorded in the long delay time range of 0–78.6 μs and (c) in the short delay time range of 0–309 ns. Decay traces at 470 nm of **DtBuCzB** in the presence of **DMAP** (50 eq.) in toluene: (b) long delay time range and (d) short delay time range. c [**DtBuCzB**] $= 2.0 \times 10^{-5}$ M, $\lambda_{ex} = 355$ nm, 20 °C.

because it re-binds with **DMAP** quite easily, as indicated by the decay trace at 465 nm in Fig. 8a. The rebinding process has a time constant of 13.9 μs under our specific experimental conditions (Fig. 8b). This time scale agrees with the molecular diffusion kinetics in fluid solution at room temperature. It is worth mentioning that the time required for recombination depends on the experimental conditions, such as the concentration of **DMAP**, the temperature, the solvent viscosity, *etc.* (Table S1†).

At the short time scale, the ns-TA spectra of **DtBuCzB** in the presence of an excess of **DMAP** show an ESA band centered at 465 nm and a negative band centered at 486 nm, due to stimulated emission (Fig. 8c), similar to the last spectral component in the fs TA spectra (Fig. 6a). The kinetic trace at 470 nm shows a rise component of 86 ns, which indicates the time needed for complete adduct dissociation (Fig. 8d). Previously, the photodissociation of the Lewis acid–base adduct of a planarized trinaphthylborane with a partially fused structure and pyridine was studied with fluorescence spectra, and the re-binding of the photo-generated borane with pyridine was observed, but it was not monitored with ns-TA spectroscopy.[75] Recently the binding of **DtBuCzB** or the dioxygen-bridged analogues with F^- anions, **DMAP** or pyridine, was studied with steady state UV-vis absorption and fluorescence spectra, but not with transient absorption spectra.[74,78] We also studied the adduct of **DtBuCzB** with F^- anions with ns-TA spectra (data not shown here), and no photodissociation was observed.

To confirm the occurrence of photodissociation and rebinding, we studied the ns-TA spectra of the **DtBuCzB-DMAP** mixture in viscous solvents, such as in toluene/silicone oil mixed solution. We obtained similar ns-TA spectra (Fig. S23†), observing a 109 ns rise phase for the kinetic trace at 470 nm, followed by a decay occurring in *ca.* 17.9 μs (Fig. S28†). These results agree with the expected retarded photo-dissociation as well as the subsequent slower re-binding in a viscous solvent. We also studied the ns-TA spectra of the **DtBuCzB-DMAP** mixture in the polar solvent acetonitrile, and the results are very similar to those in toluene. In this case, the rise phase of the kinetic trace at 470 nm takes 58 ns, while the decay occurs in 4.5 μs (Fig. S33†). It was furthermore shown that in a polymer film, the relaxation of the S_1 state is slower by 3–4 fold as compared to that in fluid solution.[64]

Time-resolved electron paramagnetic resonance (TREPR) spectral study: character of the triplet excited state of the MRE TADF emitters. It is important to unveil the triplet exciton properties of the TADF emitters based on the MRE, for instance, the electron spin selectivity of the ISC of this type of novel emitter and the spatial delocalization of the triplet excited state wave function, *i.e.* the average electron–electron distance of the two unpaired spins of the triplet excited state. Optical spectroscopy can hardly supply this information, while pulsed laser excited continuous wave (CW) TREPR spectroscopy is particularly useful because it directly accesses the electron spin–spin dipolar interaction magnitude, manifested by the ZFS *D* and *E* parameters.[1,26,28,86]

Moreover, the electron spin selectively of the ISC is manifested by the electron spin polarization (ESP) pattern of the triplet state TREPR spectrum, *i.e.* either the enhanced absorption or the emission features in the canonical orientation of the molecules in the magnetic field.

Previously, TREPR spectroscopy has been used to characterize the conventional electron D–A dyad TADF emitters.[27,29,56,57,59] The triplet states of the two possible representative MRE TADF emitters **DABNA-1** and **DtBuCzB**, were studied with TREPR spectroscopy in a frozen solution at 80 K (Fig. 9). For **DABNA-1** and **DtBuCzB**, a polarized transient TREPR spectrum with E/A features (E: emissive; A: enhanced absorptive) was observed (Fig. 9a and b). Only one triplet was observed regardless of the concentration of these compounds. The spectra of the two compounds slightly differ due to different polarizations, but the parameter *D* is equal to 1450 MHz for both compounds, and $E = -264$ MHz and -200 MHz, respectively (Table 3).

We also recorded the TREPR spectra of the compounds upon binding with **DMAP** (Fig. 9c and d). Interestingly, the TREPR spectrum of the **DABNA/DMAP** adduct corresponds to one type of triplet state (Fig. 9c), and simulations indicate that the ZFS *D*

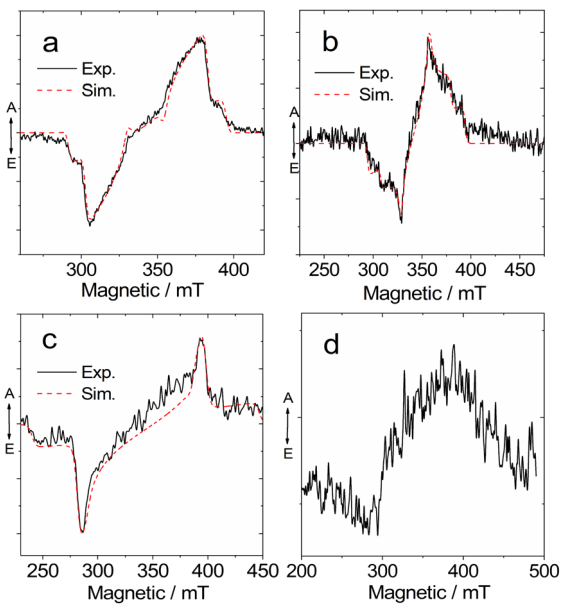

Fig. 9 Experimental and simulation TREPR spectra of (a) **DABNA-1**, (b) **DtBuCzB** in toluene/2-MeTHF (1 : 1), (c) **DABNA-1** + 50 eq. **DMAP**, and (d) **DtBuCzB** + 50 eq. **DMAP**. At 80 K. *c* [**DABNA-1**] = 5.0×10^{-4} M, *c* [**DtBuCzB**] = 5.0×10^{-4} M, the laser energy is 1 mJ per pulse at 355 nm. The delay after laser flash (DAF) is 300 ns.

Table 3 ZFS parameters (*D* and *E*) and relative population rates *Px*, *y*, and *z* of the zero-field spin states of **DABNA-1** and **DtBuCzB**[a]

Sample	*D*/MHz	*E*/MHz	*Px*	*Py*	*Pz*	*g*-Factor
DABNA-1	1450	−264	0.83	0.17	0	2.007
DtBuCzB	1450	−200	0.44	056	0	
DABNA-1+DMAP	2900	−116	0.8	0.2	0	

[a] Obtained from simulation of the triplet-state TREPR spectra of the indicated molecules in toluene/2-MeTHF (1 : 1, v/v) at 80 K.

parameter becomes as large as 2900 MHz, while the *E* parameter is −116 MHz (Table 3). These changes are in agreement with the optical spectral studies, showing that the size of the π-conjugation framework is reduced upon binding with DMAP, because the vacant p-orbital of the center B atom is occupied upon formation of a B–N dative bond.[87,88] At 80 K the photodissociation of the **DABNA-1/DMAP** adduct is suppressed as also shown by the low temperature luminescence (Fig. 4b). A broader TREPR spectrum of weak intensity was observed for **DtBuCzB** upon binding with **DMAP**, probably due to partial photodissociation (Fig. 9d).

Theoretical studies. Theoretical computations were performed to rationalize the optical and the electron paramagnetic resonance spectral observations. The geometries of the lowest triplet state were optimized with the unrestricted DFT method, using the B3LYP functional, and the 6-31G(d) basis set, with the Gaussian 16 program.[89]

The boron center of **DABNA-1** and **DtBuCzB** is almost planar (Fig. 10a and b), and the torsion is 11.6° and 9.9°, respectively. These geometries are close to those of the S_0 state obtained with restricted DFT (Fig. S32†). The electron spin density surfaces of the T_1 state of **DABNA-1** and **DtBuCzB** are presented in Fig. 10c and d. The electron spin density spreads over the entire π-conjugation system.

To better characterize the triplet state of the B–N compounds, further calculations involving spin–orbit coupling and wavefunction based methods (ROHF = restricted open shell Hartree Fock, CIS = configuration interaction singles, CASSCF = complete active space self consistent field, and NEVPT2 = N-Electron Valence State Perturbation Theory[90]) were performed with the ORCA programs[91,92] employing the def2-SVP basis and in some cases also the def2-TZVP basis. To reduce the computational cost, the *t*-butyl groups of **DtBuCzB** were replaced by hydrogen atoms, and this compound was called **CzB-H**. To check how much the phenyl groups are involved in the electronic excitations in **DABNA-1**, we also considered **DABNA-H** where these phenyl groups are replaced by hydrogen atoms, as shown in Scheme 1.

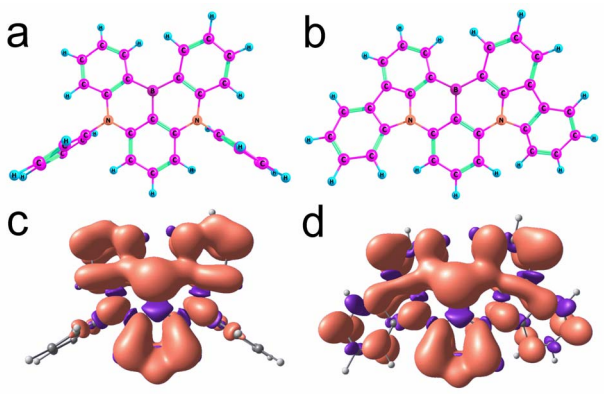

Fig. 10 The optimized T_1 state geometry of (a) **DABNA-1** and (b) **CzB-H**, and the electron spin-density surfaces of the T_1 state of **DABNA-1** (c) and **CzB-H** (d). Calculations with the UB3LYP/def2-SVP method.

Table 4 Calculated ZFS parameters *D* and *E* (absolute values) with different methods

	UB3LYP/def2-SVP		ROHF/def2-TZVP	
Compounds	*D*/MHz	*E*/MHz	*D*/MHz	*E*/MHz
DABNA-H	1437	164	1746	498
DABNA-1	1438	162	1738	471
CzB-H[a]	1254	153	1455	223
CzB-H[b]	1246	150	1453	218

[a] C_2 symmetry. [b] C_S symmetry.

The Zero Field Splitting (ZFS) parameters *D* and *E* for the T_1 state were computed from UB3LYP/def2-SVP geometry optimizations as well as ROHF/def2-TZVP calculations at these optimized geometries. In contrast to ROHF, UB3LYP suffers from spin contamination (spin angular momentum S^2 = *ca.* 2.015). However, geometries cannot be optimized with ROHF since no gradients are implemented in ORCA. The results are summarized in Table 4.

The optimized geometries of **DABNA-H** and **DABNA-1** have C_2 symmetry. For **CzB-H** we find two stable conformers with C_2 and C_S symmetry, respectively, with almost the same energies. The calculated values from UB3LYP agree very well with the experimental data, whereas ROHF overestimates the value of *D* by *ca.* 20%. The variation of the ZFS *D* parameter from **DABNA-1** to **CzB-H** agrees with the increased spin delocalization in **DtBuCzB**, for which the π-conjugation system is larger than that of **DABNA-1**.

The electronically excited states of **DABNA-1** have been previously studied. Methods which consider single electron excitations only, like TD-DFT or CIS, predict energy gaps between S_1 and T_1 of *ca.* 0.5 eV which is much larger than the experimental values (*ca.* 0.15 eV) obtained from the fluorescence and phosphorescence spectra. Hall *et al.* showed the SCS-CC2 method, which considers correlation through doubly excited configurations, could precisely predict the S_1/T_1 state energy gap.[66] The reason is that the Coulomb correlation effects are substantially larger in the lowest singlet excited state compared to the corresponding triplet. These calculations also confirmed the short-range CT nature of the S_1 and T_1 states of the MRE emitters.[66] When dynamic correlation is considered in the theoretical method, *e.g.* in SCS-CC2 or CASSCF+NEVPT2, the S_2 and T_2 states appear much higher in energy. Hence these states should not be involved in ISC and rISC required for TADF. This is different from the calculation results reported previously.[93]

We used CASSCF(10|10) in combination with NEVPT2 to obtain the energy gap between S_1 and T_1 states. For **DABNA-H** and **DABNA-1** the CASSCF was averaged over three singlet and two triplet states. A third triplet had to be included for **CzB-H** since at the CASSCF level the lowest three triplets are almost degenerate. In accordance with the observations of Hall *et al.*, the second order perturbation correction by NEVPT2 lowers S_1 much more than T_1, bringing both states close together. With the def2-SVP basis the gap is 0.192 eV for **DABNA-H**, 0.105 eV for

DABNA-1, and 0.068 eV for **CzB-H**. Similar values are obtained with the larger def2-TZVP basis, namely 0.18 eV, 0.075 eV, and 0.170 eV, respectively. In addition, S_2 and T_2 are shifted to higher energies, making S_1 and T_1 the only relevant states for TADF.

Since the experimental small S_1/T_1 state energy gaps are confirmed by these calculations, the absence of TADF in solution must be due to a small ISC rate. ISC rate constants can be calculated with the ESD[94,95] (excited states dynamics) module implemented in ORCA. However, consideration of the vibronic interactions (Herzberg–Teller terms) is only possible with single reference methods like TD-DFT or CIS. Inspection of the CASSCF wavefunctions shows that these are dominated by the HOMO–LUMO configuration, and that NEVPT2 results in an energy correction that is smaller than 1% of the total energy. It is hence reasonable to assume that the CIS wavefunction is a good approximation of the CASSCF wavefunction. We optimized the geometries of S_1 and T_1 with CIS/def2-SVP for **DABNA-H**, calculated the hessians of both states, and the derivatives of the spin–orbit coupling along all normal coordinates. These data were input into a home-written program that implements the formulae of Baiardi[96] for the ISC rate constants. Fig. 11 shows the ISC and rISC rate constants between T_1 and S_1 as a function of the energy gap. At an experimental energy gap of *ca.* 1200 cm^{-1} the calculated rates are 7.6×10^6 s^{-1} and 3.1×10^4 s^{-1} for ISC and rISC, respectively. At the calculated energy gap (0.18 eV, CAS(10|10)+NEVPT2/def2-TZVP) the rates of k_{ISC} and k_{rISC} are 9.4×10^6 s^{-1} and 2.3×10^4 s^{-1}. Shizu and Kaji found very small rates for k_{ISC} and k_{rISC} ($T_1 \rightarrow S_1$); therefore the T_2 state was considered as an intermediate.[93] However, there is no experimental evidence that this T_2 state is really near enough to T_1 to allow thermal back population. In fact, our rate constant for k_{rISC} along $T_1 \rightarrow S_1$ is in good agreement with the experimental result (1.0×10^4 s^{-1}). The calculated rate for k_{ISC} is *ca.* 10% of the decay rate of spontaneous fluorescence, which explains the observed quantum yield of 88% very well. We conclude that the absence of TADF for **DABNA-1** in solution[40] is due to the rather small spin–orbit coupling between S_1 and T_1. This is in agreement with our experimental results. The difference between fluorescence and phosphorescence suggests an energy gap of 0.18 eV for **DABNA-1** and 0.14 eV for **DtBuCzB**.

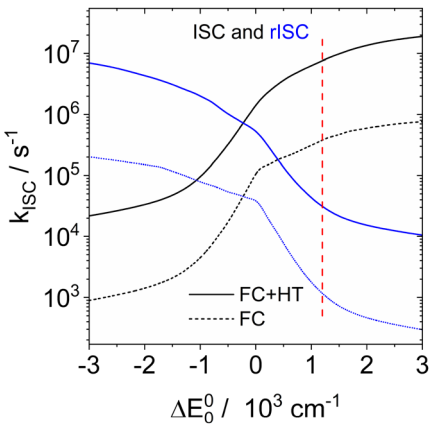

Fig. 11 ISC (black curve) and rISC (blue curve) rate constants of DABNA-H calculated with CIS/def2-SVP wavefunctions for the optimized geometries of S_1 and T_1, as a function of the energy gap. The dashed line is the Franck–Condon contribution, and the solid line includes Herzberg–Teller coupling. The vertical line marks an experimental energy gap of 1200 cm^{-1}.

The MRE idea claims that the positioning of boron and nitrogen atoms as substituents to benzene rings with a relative ortho-arrangement will localize the HOMO and LUMO on different atoms, thus reducing the exchange integral for this pair of atoms. We tested this idea by calculating the exchange integral from the difference of the expectation values of the energies for the HOMO–LUMO singlet and triplet configuration based on the orbitals obtained from the electronic ground state calculated with RHF/def2-SVP. We obtain an energy gap (*i.e.* twice the exchange integral) between these two configurations of 0.766 eV for **DABNA-H**, 0.765 eV for **DABNA-1**, and 0.543 eV for **CzB-H**. These values are too large for a TADF compound.

Mixing of many singly excited configurations *e.g.*, by the CIS or TD-DFT methods yields similar energy gaps. Apparently, the TADF properties of these compounds cannot be traced to

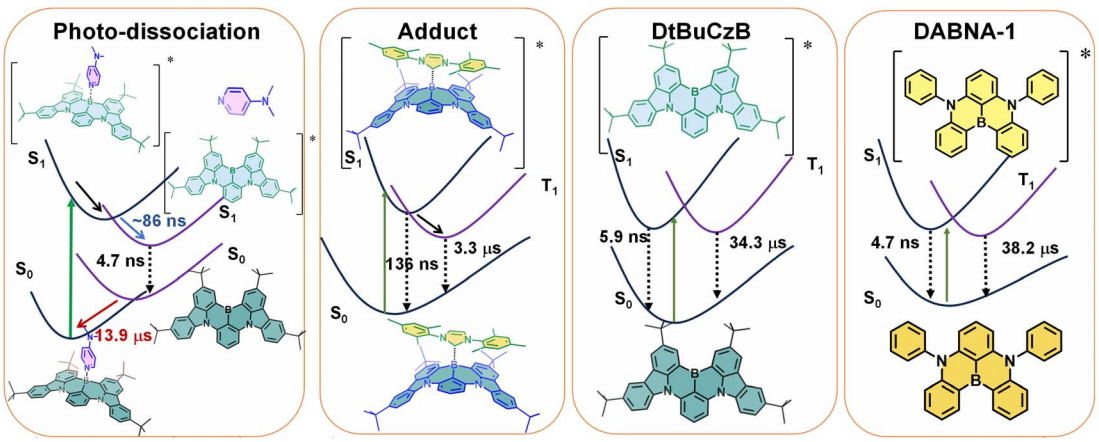

Scheme 2 Simplified Jablonski diagram illustrating the photophysical processes involved in DtBuCzB-DMAP, DtBuCzB-NHC, DtBuCzB and DABNA-1 upon photoexcitation.

a small exchange integral. Hall *et al.*[66] showed that the energy gaps of these compounds become small when correlations involving doubly and higher excited configurations are included with the SCS-CC2 method. We confirm this conclusion by CASSCF-NEVPT2 calculations. It will hence be very interesting to understand why the MRE design principle proposed by Hatakeyama[37] results in the correct prediction of good candidates for TADF although the original idea of small exchange integrals is not confirmed. Based on the above results, the photophysical process of MRE TADF molecules are summarized in Scheme 2.

Conclusions

We studied the photophysics of two representative thermally activated delayed fluorescence (TADF) emitters (**DABNA-1** and **DtBuCzB**) based on the multiple resonance effect (MRE), by using various steady state and transient optical and electron paramagnetic resonance (EPR) spectroscopic methods. For these MRE compounds, the electron exchange energy (J) is proposed to be small, leading to a small $\Delta E_{S_1/T_1}$ energy gap ($2J$), thus facilitating the reverse intersystem crossing (rISC) and TADF. Previous theoretical computations suggested that the lowest excited state of these compounds has short range charge separation character, with the HOMO and LUMO localized on different atoms in the molecular structure.

Spectral studies do not show charge transfer absorption bands, and the fluorescence is independent of the solvent polarity. These features are drastically different from the conventional charge transfer (CT) states in the D–A TADF emitters which contain separate electron donor and acceptor units. A long-lived triplet state ($\tau_T = 38.2$ μs and 34.3 μs, $\Phi_\Delta =$ 1% and 10%) was observed for these compounds in fluid solution at room temperature; however, no significant TADF was reported. Our computations show that the slow ISC is due to small SOC and small Herzberg–Teller coupling, which rationalizes the lack of TADF although the S_1/T_1 energy gap is small (0.14 eV). We found that the boron atom in these compounds behaves like a planar Lewis acidic centre and can bind with a Lewis base, such as 4-dimethylaminopyridine (**DMAP**) and a representative *N*-heterocyclic carbene (**NHC**). **DtBuCzB** shows a higher binding constant with **DMAP** [$(4.51 \pm 0.007) \times 10^3$ M^{-1}] and **NHC** [$(5.06 \pm 0.03) \times 10^3$ M^{-1}], in comparison to the binding of **DABNA-1** with **DMAP** [$(1.06 \pm 0.001) \times 10^2$ M^{-1}]. Upon photoexcitation, photo-dissociation of the **DMAP** adduct occurs and fluorescence from the photo-released native **DABNA-1** or **DtBuCzB** is observed. Photodissociation was confirmed by femtosecond and nanosecond transient absorption (fs/ns-TA) spectroscopy. The dissociation process is slow, taking about 86 ns for completeness. Subsequent re-binding of the MRE molecules with **DMAP** was observed, which takes *ca.* 14 μs under our specific experimental conditions, indicating that it is a diffusion-controlled process. No photodissociation was observed for the adduct of **DtBuCzB** with **NHC**, which emits at 383 nm (the pristine **DtBuCzB** emits at 481 nm). Interestingly, for the **DtBuCzB/NHC** and **DABNA-1/NHC** adducts, TADF was observed at room temperature (the delayed fluorescence lifetimes are $\tau_{DF} = 136$ ns and 127 ns). The triplet excited state of the TADF emitters based on the MRE was also studied by time-resolved electron paramagnetic resonance (TREPR) spectroscopy. The triplet states of the free MRE molecules are characterized by the same parameter D but differ in the degree of orthorhombic distortion. Upon binding of **DABNA-1** with **DMAP**, an increased ZFS D parameter is observed which agrees with the reduced π-conjugation upon binding. These in-depth photophysical studies are helpful for understanding the mechanism of the TADF emitters based on the MRE, as well as for study of fundamental photochemistry of triplet excited states.

Data availability

All relevant data are presented in the main text and/or ESI.†

Author contributions

X. Chen, L. Sun, A. A. Sukhanov and S. Doria contributed equally to this work; J. Zhao conceived the research, directed the analysis of the results; X. Chen, L. Sun and H. Xu synthesized the materials; X. Chen performed the UV-vis absorption, fluorescence and nanosecond transient absorption studies and performed parts of the data analysis; A. A. Sukhanov and V. K. Voronkova did the TREPR spectral studies and analyzed the data; S. Doria, L. Bussotti and M. Di Donato did the femtosecond transient absorption studies and analyzed the data; B. Dick performed the calculations with wavefunction based methods and of the ISC rate constants, using ORCA program and analyzed the data; J. Zhao, H. Xu, B. Dick, V. K. Voronkova and M. D. Donato wrote the manuscript.

Conflicts of interest

There are no conflicts to declare.

Acknowledgements

J. Z. thanks the National Key Research and Development Program of China (the Ministry of Science and Technology, No. 2023YFE0197600), the NSFC (U2001222), the Research and Innovation Team Project of the Dalian University of Technology (DUT2022TB10), the Fundamental Research Funds for the Central Universities (DUT22LAB610) and the State Key Laboratory of Fine Chemicals for financial support. H. X. thanks the Open Research Fund of the School of Chemistry and Chemical Engineering of Henan Normal University for financial support. A. A. S. and V. K. V. acknowledge financial support from the government assignment for the FRC Kazan Scientific Centre of RAS. M. D. D. thanks the European Union's Horizon 2020 Research and Innovation Program under grant agreement n. 871124 Laser lab-Europe for the support. Lei Sun is grateful for the funding of Postgraduate Research & Practice Innovation Program of Jiangsu Province (No. KYCX23_1167).

Notes and references

1 J. W. Verhoeven, *J. Photochem. Photobiol., C*, 2006, **7**, 40–60.
2 S. Fukuzumi, *Pure Appl. Chem.*, 2007, **79**, 981–991.
3 A. Devižis, J. De Jonghe-Risse, R. Hany, F. Nüesch, S. Jenatsch, V. Gulbinas and J.-E. Moser, *J. Am. Chem. Soc.*, 2015, **137**, 8192–8198.
4 A. N. Bartynski, M. Gruber, S. Das, S. Rangan, S. Mollinger, C. Trinh, S. E. Bradforth, K. Vandewal, A. Salleo, R. A. Bartynski, W. Bruetting and M. E. Thompson, *J. Am. Chem. Soc.*, 2015, **137**, 5397–5405.
5 Y. Xu, J. Zheng, J. O. Lindner, X. Wen, N. Jiang, Z. Hu, L. Liu, F. Huang, F. Würthner and Z. Xie, *Angew. Chem., Int. Ed.*, 2020, **59**, 10363–10367.
6 S. Fukuzumi, H. Kotani, K. Ohkubo, S. Ogo, N. V. Tkachenko and H. Lemmetyinen, *J. Am. Chem. Soc.*, 2004, **126**, 1600–1601.
7 O. Kei and F. Shunichi, *Bull. Chem. Soc. Jpn.*, 2009, **82**, 303–315.
8 S.-L. Meng, C. Ye, X.-B. Li, C.-H. Tung and L.-Z. Wu, *J. Am. Chem. Soc.*, 2022, **144**, 16219–16231.
9 J. Zhou, P. Chen, X. Wang, Y. Wang, Y. Wang, F. Li, M. Yang, Y. Huang, J. Yu and Z. Lu, *Chem. Commun.*, 2014, **50**, 7586–7589.
10 L.-S. Cui, H. Nomura, Y. Geng, J. U. Kim, H. Nakanotani and C. Adachi, *Angew. Chem., Int. Ed.*, 2017, **56**, 1571–1575.
11 M. Y. Wong and E. Zysman-Colman, *Adv. Mater.*, 2017, **29**, 1605444.
12 Z. Yang, Z. Mao, Z. Xie, Y. Zhang, S. Liu, J. Zhao, J. Xu, Z. Chi and M. P. Aldred, *Chem. Soc. Rev.*, 2017, **46**, 915–1016.
13 Y. Im, S. Y. Byun, J. H. Kim, D. R. Lee, C. S. Oh, K. S. Yook and J. Y. Lee, *Adv. Funct. Mater.*, 2017, **27**, 1603007.
14 F. B. Dias, T. J. Penfold and A. P. Monkman, *Methods Appl. Fluoresc.*, 2017, **5**, 012001.
15 P. L. dos Santos, M. K. Etherington and A. P. Monkman, *J. Mater. Chem. C*, 2018, **6**, 4842–4853.
16 X. Cai and S.-J. Su, *Adv. Funct. Mater.*, 2018, **28**, 1802558.
17 T. Huang, W. Jiang and L. Duan, *J. Mater. Chem. C*, 2018, **6**, 5577–5596.
18 M.-Y. Leung, M.-C. Tang, W.-L. Cheung, S.-L. Lai, M. Ng, M.-Y. Chan and V. Wing-Wah Yam, *J. Am. Chem. Soc.*, 2020, **142**, 2448–2459.
19 Y. Xu, P. Xu, D. Hu and Y. Ma, *Chem. Soc. Rev.*, 2021, **50**, 1030–1069.
20 Y.-Z. Shi, H. Wu, K. Wang, J. Yu, X.-M. Ou and X.-H. Zhang, *Chem. Sci.*, 2022, **13**, 3625–3651.
21 B. D. Dherange, M. Yuan, C. B. Kelly, C. A. Reiher, C. Grosanu, K. J. Berger, O. Gutierrez and M. D. Levin, *J. Am. Chem. Soc.*, 2023, **145**, 17–24.
22 W.-K. Kwok, L.-K. Li, S.-L. Lai, M.-Y. Leung, W. K. Tang, S.-C. Cheng, M.-C. Tang, W.-L. Cheung, C.-C. Ko, M.-Y. Chan and V. W.-W. Yam, *J. Am. Chem. Soc.*, 2023, **145**, 9584–9595.
23 H. Tanaka, K. Shizu, H. Miyazaki and C. Adachi, *Chem. Commun.*, 2012, **48**, 11392–11394.
24 H. Uoyama, K. Goushi, K. Shizu, H. Nomura and C. Adachi, *Nature*, 2012, **492**, 234–238.
25 D. M. E. Freeman, A. J. Musser, J. M. Frost, H. L. Stern, A. K. Forster, K. J. Fallon, A. G. Rapidis, F. Cacialli, I. McCulloch, T. M. Clarke, R. H. Friend and H. Bronstein, *J. Am. Chem. Soc.*, 2017, **139**, 11073–11080.
26 Y. Hou, X. Zhang, K. Chen, D. Liu, Z. Wang, Q. Liu, J. Zhao and A. Barbon, *J. Mater. Chem. C*, 2019, **7**, 12048–12074.
27 G. Tang, A. A. Sukhanov, J. Zhao, W. Yang, Z. Wang, Q. Liu, V. K. Voronkova, M. Di Donato, D. Escudero and D. Jacquemin, *J. Phys. Chem. C*, 2019, **123**, 30171–30186.
28 X. Zhang, Z. Wang, Y. Hou, Y. Yan, J. Zhao and B. Dick, *J. Mater. Chem. C*, 2021, **9**, 11944–11973.
29 X. Zhang, X. Liu, M. Taddei, L. Bussotti, I. Kurganskii, M. Li, X. Jiang, L. Xing, S. Ji, Y. Huo, J. Zhao, M. Di Donato, Y. Wan, Z. Zhao and M. V. Fedin, *Chem.–Eur. J.*, 2022, **28**, e202200510.
30 X. Zhao and J. Zhao, *Chem. Commun.*, 2022, **58**, 7666–7669.
31 X. Zhao, A. A. Sukhanov, X. Jiang, J. Zhao and V. K. Voronkova, *J. Phys. Chem. Lett.*, 2022, **13**, 2533–2539.
32 X. Zhang, X. Zhao, K. Ye and J. Zhao, *Chem.–Eur. J.*, 2023, **29**, e202203737.
33 M. K. Etherington, J. Gibson, H. F. Higginbotham, T. J. Penfold and A. P. Monkman, *Nat. Commun.*, 2016, **7**, 13680.
34 X. Cao, D. Zhang, S. Zhang, Y. Tao and W. Huang, *J. Mater. Chem. C*, 2017, **5**, 7699–7714.
35 L. Chen, W.-C. Chen, Z. Yang, J.-H. Tan, S. Ji, H.-L. Zhang, Y. Huo and C.-S. Lee, *J. Mater. Chem. C*, 2021, **9**, 17233–17264.
36 H. Hirai, K. Nakajima, S. Nakatsuka, K. Shiren, J. Ni, S. Nomura, T. Ikuta and T. Hatakeyama, *Angew. Chem., Int. Ed.*, 2015, **54**, 13581–13585.
37 T. Hatakeyama, K. Shiren, K. Nakajima, S. Nomura, S. Nakatsuka, K. Kinoshita, J. Ni, Y. Ono and T. Ikuta, *Adv. Mater.*, 2016, **28**, 2777–2781.
38 S. Oda, B. Kawakami, R. Kawasumi, R. Okita and T. Hatakeyama, *Org. Lett.*, 2019, **21**, 9311–9314.
39 I. Kim, K. H. Cho, S. O. Jeon, W.-J. Son, D. Kim, Y. M. Rhee, I. Jang, H. Choi and D. S. Kim, *JACS Au*, 2021, **1**, 987–997.
40 X. Wu, B.-K. Su, D.-G. Chen, D. Liu, C.-C. Wu, Z.-X. Huang, T.-C. Lin, C.-H. Wu, M. Zhu, E. Y. Li, W.-Y. Hung, W. Zhu and P.-T. Chou, *Nat. Photonics*, 2021, **15**, 780–786.
41 J.-K. Li, X.-Y. Chen, Y.-L. Guo, X.-C. Wang, A. C. H. Sue, X.-Y. Cao and X.-Y. Wang, *J. Am. Chem. Soc.*, 2021, **143**, 17958–17963.
42 J. Eng and T. J. Penfold, *Commun. Chem.*, 2021, **4**, 91.
43 Q. Ou, Y. Shao and Z. Shuai, *J. Am. Chem. Soc.*, 2021, **143**, 17786–17792.
44 I. S. Park, H. Min and T. Yasuda, *Angew. Chem., Int. Ed.*, 2022, **61**, e202205684.
45 X. Cao, K. Pan, J. Miao, X. Lv, Z. Huang, F. Ni, X. Yin, Y. Wei and C. Yang, *J. Am. Chem. Soc.*, 2022, **144**, 22976–22984.
46 S. Oda, B. Kawakami, Y. Yamasaki, R. Matsumoto, M. Yoshioka, D. Fukushima, S. Nakatsuka and T. Hatakeyama, *J. Am. Chem. Soc.*, 2022, **144**, 106–112.

47 Y. Sano, T. Shintani, M. Hayakawa, S. Oda, M. Kondo, T. Matsushita and T. Hatakeyama, *J. Am. Chem. Soc.*, 2023, **145**, 11504–11511.
48 S. Uemura, S. Oda, M. Hayakawa, R. Kawasumi, N. Ikeda, Y.-T. Lee, C.-Y. Chan, Y. Tsuchiya, C. Adachi and T. Hatakeyama, *J. Am. Chem. Soc.*, 2023, **145**, 1505–1511.
49 M. Yang, I. S. Park and T. Yasuda, *J. Am. Chem. Soc.*, 2020, **142**, 19468–19472.
50 Y. Liu, X. Xiao, Z. Huang, D. Yang, D. Ma, J. Liu, B. Lei, Z. Bin and J. You, *Angew. Chem., Int. Ed.*, 2022, **61**, e202210210.
51 J. M. dos Santos, D. Sun, J. M. Moreno-Naranjo, D. Hall, F. Zinna, S. T. J. Ryan, W. Shi, T. Matulaitis, D. B. Cordes, A. M. Z. Slawin, D. Beljonne, S. L. Warriner, Y. Olivier, M. J. Fuchter and E. Zysman-Colman, *J. Mater. Chem. C*, 2022, **10**, 4861–4870.
52 T. Hosokai, H. Matsuzaki, A. Furube, K. Tokumaru, T. Tsutsui, H. Nakanotani, M. Yahiro and C. Adachi, *SID Symposium Digest of Technical Papers*, 2016, vol. 47, pp. 786–789.
53 J. Choi, D.-S. Ahn, K. Y. Oang, D. W. Cho and H. Ihee, *J. Phys. Chem. C*, 2017, **121**, 24317–24323.
54 W. Zhang, H. Song, J. Kong, Z. Kuang, M. Li, Q. Guo, C.-f. Chen and A. Xia, *J. Phys. Chem. C*, 2019, **123**, 19322–19332.
55 Y. Guo, Y. Gao, J. Zhang, C. Wang, Y. Wang, X. Feng and G. Zhao, *J. Phys. Chem. C*, 2023, **127**, 4784–4791.
56 T. Ogiwara, Y. Wakikawa and T. Ikoma, *J. Phys. Chem. A*, 2015, **119**, 3415–3418.
57 E. W. Evans, Y. Olivier, Y. Puttisong, W. K. Myers, T. J. H. Hele, S. M. Menke, T. H. Thomas, D. Credgington, D. Beljonne, R. H. Friend and N. C. Greenham, *J. Phys. Chem. Lett.*, 2018, **9**, 4053–4058.
58 N. Sharma, M. Y. Wong, D. Hall, E. Spuling, F. Tenopala-Carmona, A. Privitera, G. Copley, D. B. Cordes, A. M. Z. Slawin, C. Murawski, M. C. Gather, D. Beljonne, Y. Olivier, I. D. W. Samuel and E. Zysman-Colman, *J. Mater. Chem. C*, 2020, **8**, 3773–3783.
59 B. H. Drummond, N. Aizawa, Y. Zhang, W. K. Myers, Y. Xiong, M. W. Cooper, S. Barlow, Q. Gu, L. R. Weiss, A. J. Gillett, D. Credgington, Y.-J. Pu, S. R. Marder and E. W. Evans, *Nat. Commun.*, 2021, **12**, 4532.
60 Y. Kobori, M. Fuki and H. Murai, *J. Phys. Chem. B*, 2010, **114**, 14621–14630.
61 N. Zarrabi, B. J. Bayard, S. Seetharaman, N. Holzer, P. Karr, S. Ciuti, A. Barbon, M. Di Valentin, A. van der Est, F. D'Souza and P. K. Poddutoori, *Phys. Chem. Chem. Phys.*, 2021, **23**, 960–970.
62 X. Xiao, I. Kurganskii, P. Maity, J. Zhao, X. Jiang, O. F. Mohammed and M. Fedin, *Chem. Sci.*, 2022, **13**, 13426–13441.
63 Y. Xu, Z. Cheng, Z. Li, B. Liang, J. Wang, J. Wei, Z. Zhang and Y. Wang, *Adv. Opt. Mater.*, 2020, **8**, 1902142.
64 Y. Gao, Y. Wang, Z. Guo, Y. Wan, C. Li, B. Yang, W. Yang and X. Ma, *J. Phys. Chem. B*, 2022, **126**, 2729–2739.
65 A. Pershin, D. Hall, V. Lemaur, J.-C. Sancho-Garcia, L. Muccioli, E. Zysman-Colman, D. Beljonne and Y. Olivier, *Nat. Commun.*, 2019, **10**, 597.
66 D. Hall, J. C. Sancho-García, A. Pershin, G. Ricci, D. Beljonne, E. Zysman-Colman and Y. Olivier, *J. Chem. Theory Comput.*, 2022, **18**, 4903–4918.
67 M. Saigo, Y. Shimoda, T. Ehara, T. Ryu, K. Miyata and K. Onda, *Bull. Chem. Soc. Jpn.*, 2022, **95**, 381–388.
68 H. Tanaka, K. Shizu, H. Nakanotani and C. Adachi, *J. Phys. Chem. C*, 2014, **118**, 15985–15994.
69 B. Valeur, *Molecular Fluorescence: Principles and Applications*, Wiley-VCH Verlag GmbH, 2001.
70 D. Hall, S. M. Suresh, P. L. dos Santos, E. Duda, S. Bagnich, A. Pershin, P. Rajamalli, D. B. Cordes, A. M. Z. Slawin, D. Beljonne, A. Köhler, I. D. W. Samuel, Y. Olivier and E. Zysman-Colman, *Adv. Opt. Mater.*, 2020, **8**, 1901627.
71 L.-S. Cui, A. J. Gillett, S.-F. Zhang, H. Ye, Y. Liu, X.-K. Chen, Z.-S. Lin, E. W. Evans, W. K. Myers, T. K. Ronson, H. Nakanotani, S. Reineke, J.-L. Bredas, C. Adachi and R. H. Friend, *Nat. Photonics*, 2020, **14**, 636–642.
72 S. Goto, Y. Nitta, N. O. Decarli, L. E. de Sousa, P. Stachelek, N. Tohnai, S. Minakata, P. de Silva, P. Data and Y. Takeda, *J. Mater. Chem. C*, 2021, **9**, 13942–13953.
73 Z. Zhou, A. Wakamiya, T. Kushida and S. Yamaguchi, *J. Am. Chem. Soc.*, 2012, **134**, 4529–4532.
74 Y. Qi, X. Cao, Y. Zou and C. Yang, *J. Mater. Chem. C*, 2021, **9**, 1567–1571.
75 K. Matsuo, S. Saito and S. Yamaguchi, *J. Am. Chem. Soc.*, 2014, **136**, 12580–12583.
76 N. Ando, T. Yamada, H. Narita, N. N. Oehlmann, M. Wagner and S. Yamaguchi, *J. Am. Chem. Soc.*, 2021, **143**, 9944–9951.
77 F.-W. Gao, R.-L. Zhong, H.-L. Xu and Z.-M. Su, *J. Phys. Chem. C*, 2017, **121**, 25472–25478.
78 G. Li, X. Liu, M. Wu, R. Zeng, Q. Li, A. Yuan and C. Shi, *Dyes Pigm.*, 2023, **208**, 110805.
79 M. Mamada, M. Hayakawa, J. Ochi and T. Hatakeyama, *Chem. Soc. Rev.*, 2024, **53**, 1624–1692.
80 Y. Kitamoto, F. Kobayashi, T. Suzuki, Y. Miyata, H. Kita, K. Funaki and S. Oi, *Dalton Trans.*, 2019, **48**, 2118–2127.
81 J. Guo, Y. Yang, C. Dou and Y. Wang, *J. Am. Chem. Soc.*, 2021, **143**, 18272–18279.
82 S.-B. Zhao, T. McCormick and S. Wang, *Inorg. Chem.*, 2007, **46**, 10965–10967.
83 Y. Sun, Z. M. Hudson, Y. Rao and S. Wang, *Inorg. Chem.*, 2011, **50**, 3373–3378.
84 C. J. Berger, G. He, C. Merten, R. McDonald, M. J. Ferguson and E. Rivard, *Inorg. Chem.*, 2014, **53**, 1475–1486.
85 M. Saigo, K. Miyata, S. i. Tanaka, H. Nakanotani, C. Adachi and K. Onda, *J. Phys. Chem. Lett.*, 2019, **10**, 2475–2480.
86 T. Biskup, *Front. Chem.*, 2019, **7**, 10.
87 H. Levanon and J. R. Norris, *Chem. Rev.*, 1978, **78**, 185–198.
88 S. Richert, C. E. Tait and C. R. Timmel, *J. Magn. Reson.*, 2017, **280**, 103–116.
89 M. J. Frisch, G. W. Trucks, H. B. Schlegel, G. E. Scuseria, M. A. Robb, J. R. Cheeseman, G. Scalmani, V. Barone, G. A. Petersson, H. Nakatsuji, X. Li, M. Caricato, A. V. Marenich, J. Bloino, B. G. Janesko, R. Gomperts, B. Mennucci, H. P. Hratchian, J. V. Ortiz, A. F. Izmaylov, J. L. Sonnenberg, D. Williams-Young, F. Ding, F. Lipparini, F. Egidi, J. Goings, B. Peng, A. Petrone, T. Henderson,

D. Ranasinghe, V. G. Zakrzewski, J. Gao, N. Rega, G. Zheng, W. Liang, M. Hada, M. Ehara, K. Toyota, R. Fukuda, J. Hasegawa, M. Ishida, T. Nakajima, Y. Honda, O. Kitao, H. Nakai, T. Vreven, K. Throssell, J. A. Montgomery Jr, J. E. Peralta, F. Ogliaro, M. J. Bearpark, J. J. Heyd, E. N. Brothers, K. N. Kudin, V. N. Staroverov, T. A. Keith, R. Kobayashi, J. Normand, K. Raghavachari, A. P. Rendell, J. C. Burant, S. S. Iyengar, J. Tomasi, M. Cossi, J. M. Millam, M. Klene, C. Adamo, R. Cammi, J. W. Ochterski, R. L. Martin, K. Morokuma, O. Farkas, J. B. Foresman and D. J. Fox, *Gaussian 16 Rev. C.01*, 2016.

90 C. Angeli, R. Cimiraglia, S. Evangelisti, T. Leininger and J.-P. Malrieu, *J. Chem. Phys.*, 2001, **114**, 10252–10264.

91 F. Neese, F. Wennmohs, U. Becker and C. Riplinger, *J. Chem. Phys.*, 2020, **152**, 224108.

92 F. Neese, *Wiley Interdiscip. Rev.: Comput. Mol. Sci.*, 2022, **12**, e1606.

93 K. Shizu and H. Kaji, *Chem. Commun.*, 2022, **5**, 53.

94 B. de Souza, F. Neese and R. Izsák, *J. Chem. Phys.*, 2018, **148**, 034104.

95 B. de Souza, G. Farias, F. Neese and R. Izsák, *J. Chem. Theory Comput.*, 2019, **15**, 1896–1904.

96 A. Baiardi, J. Bloino and V. Barone, *J. Chem. Theory Comput.*, 2013, **9**, 4097–4115.